

## Development of a new medical image compression method for optimal storage space

*Livane NGUEJIO ZEBAZE<sup>1</sup>, Ernest KIATA<sup>2</sup>, Laurent BITJOKA<sup>3</sup>*

<sup>1</sup>Université de Ngaoundéré, Laboratoire de Physique Appliquée (PAP), Cameroon

<sup>2</sup>Laboratory of Information and Communication Technologies, Protestant University of Central Africa, Yaounde, Cameroon

<sup>3</sup>Université de Ngaoundéré, Laboratoire Energie, Signal, Imagerie et Automatique (LESIA), Cameroon

Copyright © 2021 ISSR Journals. This is an open access article distributed under the **Creative Commons Attribution License**, which permits unrestricted use, distribution, and reproduction in any medium, provided the original work is properly cited.

**ABSTRACT:** Image compression is a process of reducing the number of bits needed to represent an image. The goal is to optimize storage spaces, facilitate their transmission through the network and thus promote telemedicine. Over the years, several compression algorithms have distinguished themselves by their ability to reduce the size of the image while maintaining an acceptable visual appearance. These include the JPEG standard, the JPEG2000 standard and many others. The principle of these algorithms is essentially based on the reduction wavelet coefficients according to the singularity of the image. In this article, a new approach is proposed. The goal of this approach is to zero the wavelet coefficients regardless of the singularity of the image. To achieve this goal, our algorithm segments into three fundamental parts. The first part consists in breaking down the image into sub-bands through the QWT formalism. Subsequently, in order to obtain orthogonal matrices, we break down the matrices of the recently obtained sub-bands into singular values. The objective of these matrices is to exploit the redundancy present in the image while putting most wavelet coefficients to zero without, however significantly degrading the visual aspect of the image. To close the algorithm, we apply a thresholding function to the previously obtained wavelet coefficients. The method was evaluated by computer performance criteria such as *MSE*, *PSNR*, *CR* and *IF* and by human visual system performance criteria such as *SSIM*. These criteria are used to judge the quality of the reconstructed image and the compression ratio.

**KEYWORDS:** Discrete wavelet transform, Medical image, Quaternionic wavelet transform, Image compression, Orthogonal basis, Multiresolution analysis.

### 1 INTRODUCTION

Medical imaging is a technique that brings together the means of acquiring and reproducing images of the human body. Thanks to these images, a more detailed investigation of the human system is now possible. It allows better targeting of treatments, more refined diagnoses, more effective monitoring and more reliable neurological tests. However, the amount of data generated in this sector amounts to several terabytes/year, thus saturating the transmission and storage systems [1]. One of the solutions to this problem is image compression. The main goal of image compression is to reduce the amount of data needed to describe the image while maintaining an acceptable visual appearance of the reconstructed image. The most famous compression techniques that have given the best results are those based on the discrete cosine transform (DCT), the discrete wavelet transform (DWT) and the quaternionic wavelet transform (QWT). A committee of experts is formulating a compression technique for images commonly known as JPEG. Based on DCT, this technique is ISO standardised. Its principle was developed by Guitter [2]. In this same particular context of medical imaging compression, contrary to the principle of the JPEG standard, other authors such as Lucas, Chen and Wu, after decomposing the image with DCT, performed either scalar or vector quantization and/or applied a thresholding function to compress the images [3, 4, 5]. Woods and al proposed sub-band coding to compress images [6]. In the 2000s, a new standard was developed by ISO called JPEG2000, the principle of which was developed by Ordóñez and al [7]. In the same logic, for the achievement of better results, Ruchika and several other authors

to compress images, in addition to the methods developed by Lucas, Chen and Wu, they coupled their results with an arithmetic coder [8, 9, 10, 11, 12]. Hui and Besar performed a comparative study between the JPEG standard and the JPEG2000 standard applied to chest images. They concluded that JPEG2000 provides better results in terms of reconstructed image quality and compression ratio [13]. Perumal and Rajasekaran developed a compression method combining DWT and neural networks [14]. Miaou and al used JPEG-LS to compress medical images. This is a compression method combining adaptive coding with a Huffman-like encoder [15]. Valette and al propose a new subdivision algorithm that allows simplification of any triangular mesh using DWT [16]. Benamrane and al propose a technique for still image compression using neural networks [17]. For image compression. Anandan and Sabeenian used the fast curvelet transform coupled with an arithmetic encoder [18]. Juliet and al compress images using the Ripplet transform [19]. Although the techniques listed above provide good results, they do not take into account the geometric structure of the image. To address this problem of geometric structure, Chan and al propose a new image processing scheme based on the QWT [20]. Ledoux and Joseph used QWT to compress images [21]. Madhu and Shankar performed a comparative study between CWT, DWT and QWT. They concluded that, for a better compression ratio and image quality, QWT gives a better result [22]. Admittedly, transform compression methods have been ranked among the best performing techniques for a long time. In fact, wavelets have contributed a lot to the field of digital image processing since the 1980s, so that various orthonormal wavelet bases can be constructed using multiresolution analysis. These bases are differentiated according to their ability to cancel the largest number of wavelet coefficients while respecting the visual aspect of the original image. The problem lies in the singularity of the image. If the image has a large singularity, then the number of non-zero wavelet coefficients required to reconstruct it will be large. In this paper, we propose a completely new compression scheme based on QWT and SVD. The purpose of this algorithm is to reduce the amount of bits needed for the reconstruction of an image regardless of the singularity. To achieve this objective, the algorithm is divided into three essential parts. The first part consists in breaking down the image into sub-bands by the formalism of the quaternions. Then we break down the previously obtained sub-bands into singular values. This is in order to obtain orthogonal matrices so that most wavelet coefficients can be applied independently of the singularity of the image. To close the algorithm we apply a thresholding function and Huffman coding to all wavelet coefficients obtained in the previous step.

## 2 IMAGE DECOMPOSITION USING THE QUATERNION FORMALISM

### 2.1 ALGEBRA OF QUATERNIONS

A quaternion is a number belonging to the body  $\mathbb{H}$  (body of quaternions) developed by Hamilton in 1843 and written in the form  $q = a + ib + jc + kd$  where  $i, j$  and  $k$  are abstract numbers that satisfy the following properties:

$$\begin{cases} ij = -ji = k \\ jk = -kj = i \\ ki = -ik = j \\ ijk = -1 \end{cases} \tag{1}$$

with  $i^2 = j^2 = k^2 = -1$

$\mathbb{H}$  is a non-commutative field of dimension 4  $\{1, i, j, k\}$ , This means that for any  $p, q \in \mathbb{H}$   $pq \neq qp$ . It should be noted that,  $a, b, c$  and  $d \in \mathbb{R}$ . The polar form of a quaternion can be defined by:  $q = |q|e^{i\varphi + j\theta + k\psi}$

$$\text{With } |q|^2 = a^2 + b^2 + c^2 + d^2 \text{ et } (\varphi, \theta, \psi) \in [-\pi; \pi] \times \left[-\frac{\pi}{2}; \frac{\pi}{2}\right] \times \left[-\frac{\pi}{4}; \frac{\pi}{4}\right]$$

### 2.2 QUATERNIONIC WAVELET TRANSFORM

This section deals with the decomposition of 2D images through Chan's perfect reconstruction quaternion theory and quaternionic wavelets (QWT) [22]. Unlike DWT, QWT is practically translation invariant [23]. The coefficients resulting from this decomposition are expressed in terms of amplitude and phase. The implementation of the QWT is done by considering a scalar function  $\phi$  and a parent wavelet  $\psi$  which are separable. The analytical 2D wavelet is written:

$$\begin{cases} \phi(x) = \phi(x_1)\phi(x_2) + iH\phi(x_1)\phi(x_2) + j\phi(x_1)H\phi(x_2) + kH\phi(x_1)H\phi(x_2) \\ \psi^1(x) = \phi(x_1)\psi(x_2) + iH\phi(x_1)\psi(x_2) + j\phi(x_1)H\psi(x_2) + kH\phi(x_1)H\psi(x_2) \\ \psi^2(x) = \psi(x_1)\phi(x_2) + iH\psi(x_1)\phi(x_2) + j\psi(x_1)H\phi(x_2) + kH\psi(x_1)H\phi(x_2) \\ \psi^3(x) = \psi(x_1)\psi(x_2) + iH\psi(x_1)\psi(x_2) + j\psi(x_1)H\psi(x_2) + kH\psi(x_1)H\psi(x_2) \end{cases} \quad (2)$$

where  $H$  is the Hilbert transform:

We notice that this new decomposition is similar to the complex dual-tree, as we use the same functions as the 2D dual-tree. In the end, the QWT is a finer analysis of the complex dual-tree. These functions above provide a multi-scale quaternionic analysis of the image in three separate global directions: horizontal, vertical and diagonal.

The analytical coefficients resulting from the decomposition of the image by this formalism are obtained as follows:

$$\begin{cases} \omega_{LL,j}[k] = \langle s(x), 2^{-j}\phi(2^{-j}x-k) \rangle = A_{LL,j}e^{i\phi_{LL,j}+j\theta_{LL,j}+k\psi_{LL,j}} \\ \omega_{LH,j}[k] = \langle s(x), 2^{-j}\psi^1(2^{-j}x-k) \rangle = A_{LH,j}e^{i\phi_{LH,j}+j\theta_{LH,j}+k\psi_{LH,j}} \\ \omega_{HL,j}[k] = \langle s(x), 2^{-j}\psi^2(2^{-j}x-k) \rangle = A_{HL,j}e^{i\phi_{HL,j}+j\theta_{HL,j}+k\psi_{HL,j}} \\ \omega_{HH,j}[k] = \langle s(x), 2^{-j}\psi^3(2^{-j}x-k) \rangle = A_{HH,j}e^{i\phi_{HH,j}+j\theta_{HH,j}+k\psi_{HH,j}} \end{cases} \quad (3)$$

Unlike the bi-orthogonal wavelet transform, the coefficients from the QWT are quaternionic.

The figure below, implemented by Soulard in [24], illustrates perfectly well the calculation algorithm and the link with the complex wavelet transform. This link is found with the quaternionic Fourier transform which is expressed as two complex Fourier transforms through a symplectic decomposition.

The practical implementation of this decomposition is carried out by four separable 2D filter banks, one for each cartesian component of the quaternionic coefficients.

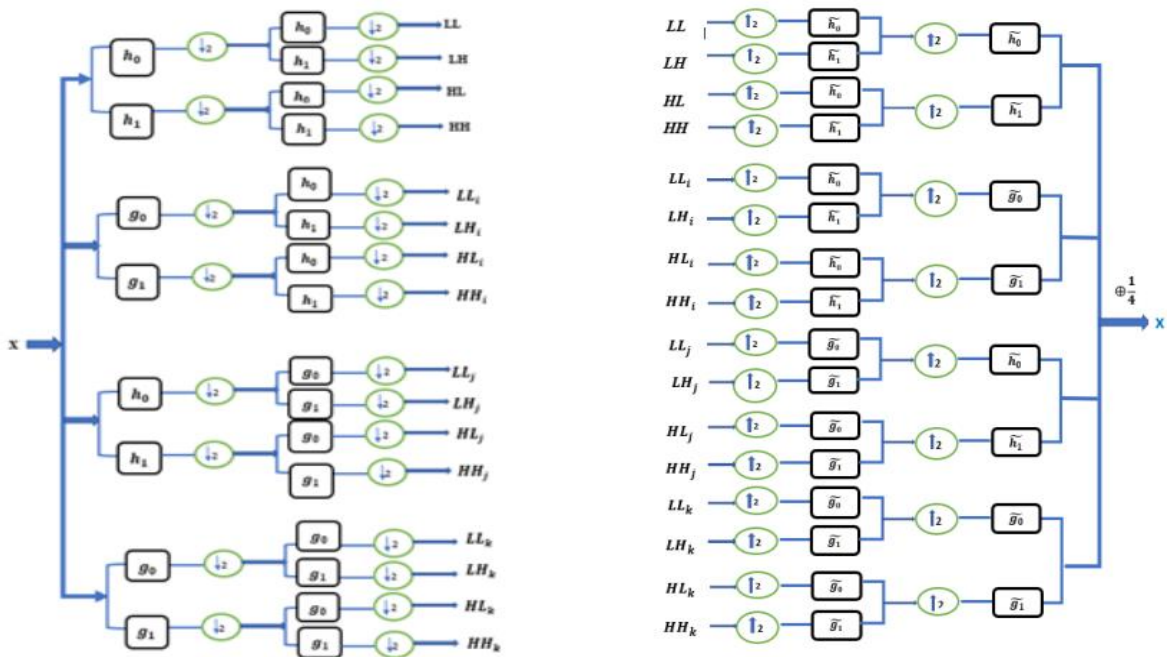


Fig. 1. 2D Decomposition and Reconstruction Structure of Quaternion Filter Banks [24].

### 3 NEW COMPRESSION ALGORITHM

The algorithm proposed in this article follows the following steps:

**Step 1:** Loading the image;

**Step 2:** Image decomposition with QWT at resolution level  $j$  with we obtain  $(3j + 1)$  elements whose matrices will be noted

$$\omega_{LL,j}, \omega_{LH,j}, \omega_{HL,j} \text{ and } \omega_{HH,j};$$

**Step 3:** We eliminate the coefficients  $\omega_{LL,j}, \omega_{LH,j}, \omega_{HL,j}$  and  $\omega_{HH,j}$  of the  $j^{th}$  of the decompositions;

**Step 4:** This step consists in reconstructing the coefficients of the sub-bands,  $\omega_{LH,j}, \omega_{HL,j}$  and  $\omega_{HH,j}$ . We obtain a new matrix

$$\text{consisting of the coefficients } \omega_{LH,j}^1, \omega_{HL,j}^1 \text{ and } \omega_{HH,j}^1;$$

**Step 5:** This stage is subdivided into several sub-stages;

— From step 4, matrices are extracted  $\omega_{LH,j}^1, \omega_{HL,j}^1$  and  $\omega_{HH,j}^1$  orthogonal matrices  $LH_{j,p}, HL_{j,p}$  and  $HH_{j,p}$ , for each even number  $p$ : The matrices  $LH_{j,p}, HL_{j,p}$  and  $HH_{j,p}$  are quaternionic values;

- Using this sub-section, we construct the orthogonal matrices  $A_{LH(j,p)}, B_{HL(j,p)}$  and  $C_{HH(j,p)}$  by making the following considerations: We choose the column vector  $N_n = (n_1, n_2, \dots, n_n)$  from  $LH_{j,p}$  which has the highest standard of  $L^1$  in relation to the other columns;
- We consider a vector  $X = (x_1, x_2, \dots, x_n)^T$  such as  $x_1 = a(a \in \mathbb{R}^*)$  and  $x_i = 0$  for  $i = 2, \dots, n$ ;

$$\bullet \text{ We let } M = XN_{N,1} \Rightarrow M = \begin{pmatrix} an_1 & an_2 & \dots & an_n \\ 0 & 0 & \dots & 0 \\ \dots & \dots & \dots & 0 \\ 0 & \dots & \dots & 0 \end{pmatrix} \tag{4}$$

- According to the principle in singular value decomposition,  $M$  can be written as  $M = U\Sigma V^*$ . Therefore, we consider  $A_{LH(j,p)} = V^*$ . Following the same logic, we determine the matrices  $B_{HL(j,p)}$  and  $C_{HH(j,p)}$  associated with the sub-bands  $HL_{j,p}$  and  $HH_{j,p}$ ;

— The new wavelet coefficients are obtained by performing the following operations:

$$\begin{cases} \omega_{LH,j}^{(11)} = A_{LH(j,p)} \omega_{LH,j}^1 \\ \omega_{HL,j}^{(12)} = B_{HL(j,p)} \omega_{HL,j}^1 \\ \omega_{HH,j}^{(11)} = C_{HH(j,p)} \omega_{HH,j}^1 \end{cases} \tag{5}$$

**Step 6:** This step involves applying a thresholding function to all new coefficients obtained in the previous step. The choice of thresholding is the soft thresholding. Unlike the hard thresholding, which always sets all coefficients below a threshold value to zero, the soft thresholding, on the other hand, for coefficients above the threshold value, attenuates the latter according to the process described by the following function:

$$\eta_s = \begin{cases} x - \lambda & \text{si } x > \lambda \\ 0 & \text{si } |x| \leq \lambda \\ x + \lambda & \text{si } x < -\lambda \end{cases} \tag{6}$$



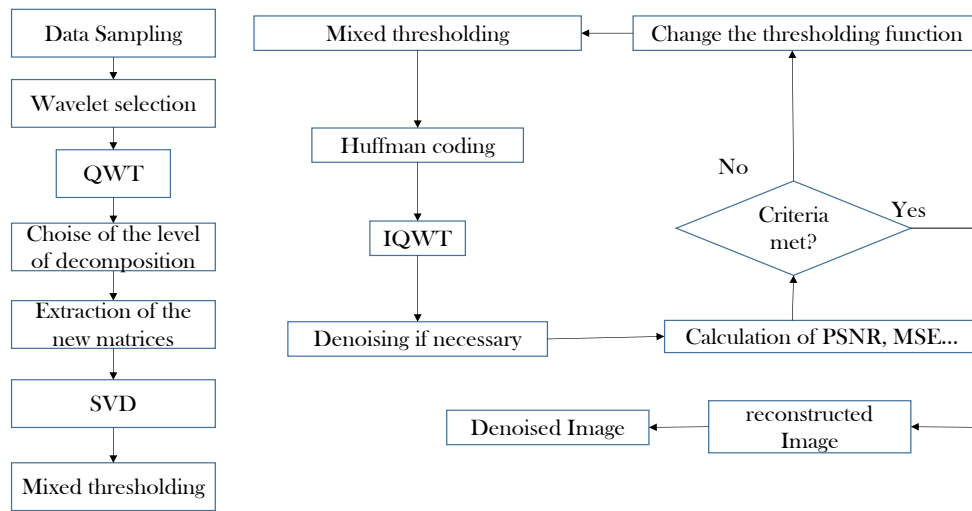


Fig. 4. Flowchart of algorithm 1.

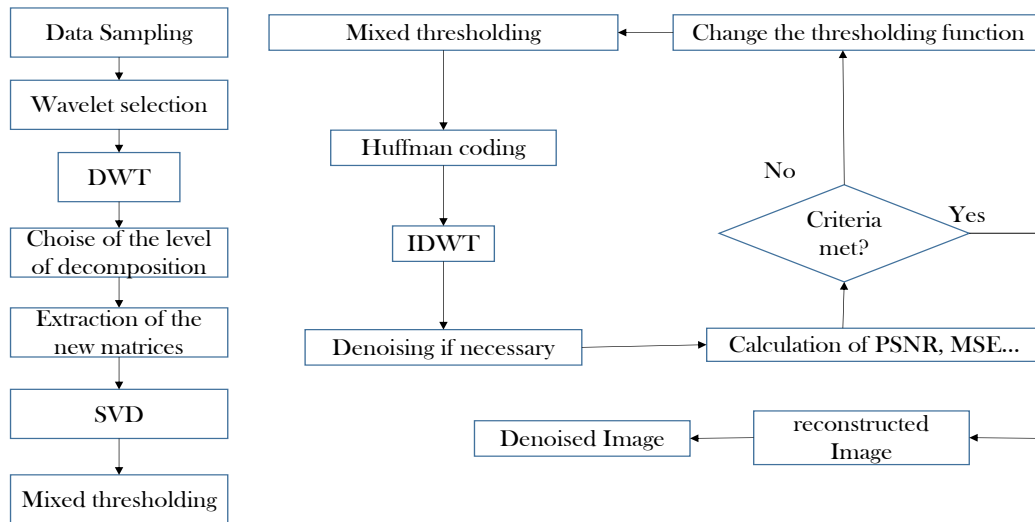


Fig. 5. Flowchart of algorithm 2

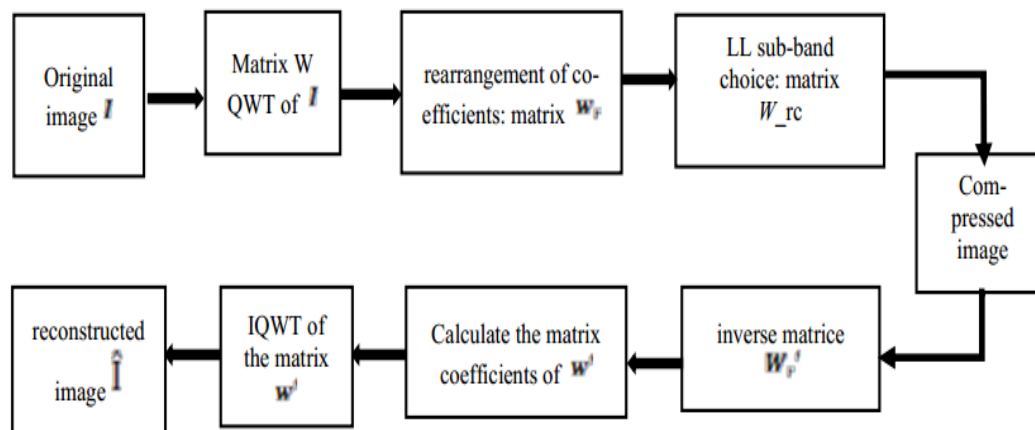


Fig. 6. Bloc diagram of algorithm 3 [21]

#### 4 EVALUATION OF PERFORMANCE CRITERIA

The evaluation of the quality of the reconstructed image at the end of the chain is based on several parameters, some of which are listed below:

- Mean Square Error ( $MSE$ ): it measures the information lost between the original image and the reconstructed image at the end of the chain. In addition, it measures the distortion between the original image and the reconstructed image after decompression. A large value of this distortion means that the image is of poor quality. This criterion is calculated as the average of the squares of the differences between the pixels of the reconstructed image and the pixels corresponding to the original image.

$$MSE^2 = \frac{1}{M \times N} \sum_{i=1}^M \sum_{j=1}^N (I(i, j) - \hat{I}(i, j))^2 \quad (6)$$

with:  $I(i, j)$  represents the original image,  $\hat{I}(i, j)$ : represents the reconstructed image.  $M$  and  $N$  are the number of rows and columns.

- Pic signal to noise ratio ( $PNSR$ ): is a factor indicating the quality of the reconstructed image in relation to the original image. A low PSNR value means that the image is of poor quality. The PSNR is calculated as follows:

$$PSNR = \log_{10} \left( \frac{\text{image\_dynamics}}{MSE} \right)^2 \quad (7)$$

- Compression ratio ( $CR$ ): It defines the gain in volume relative to the initial volume of data. It is obtained by performing the following operation:

$$CR = \left( 1 - \frac{\hat{I}(i, j)}{I(i, j)} \right) \times 100 \quad (8)$$

- Fidelity ( $IF$ ): is a parameter that evaluates the difference between the image obtained after reconstruction and the original image. A value close to 1 proves that the reconstructed image is almost identical to the original image. It is calculated as follows:

$$IF = 1 - \left( \frac{\sum_i \sum_j (I^2(i, j) - \hat{I}^2(i, j))}{\sum_i \sum_j I^2(i, j)} \right) \quad (9)$$

- Structural Similarity Index ( $SSIM$ ): This is a parameter that measures the quality of the reconstructed image. Unlike PSNR, which measures the pixel-to-pixel difference, SSIM measures the structural similarity between the original image and the reconstructed image. This parameter is obtained by the product of the luminance  $l(x, y)$ , the chrominance  $c(x, y)$  and the similarity  $s(x, y)$  therefore the relation is:

$$SSIM(x, y) = l(x, y) \cdot c(x, y) \cdot s(x, y) = \frac{\left( 2\mu_x \mu_y + c_1 \right) \left( 2\sigma_x \sigma_y + c_2 \right) \left( \text{cov}_{xy} + c_3 \right)}{\left( \mu_x^2 + \mu_y^2 + c_1 \right) \left( \sigma_x^2 + \sigma_y^2 + c_2 \right) \left( \sigma_x \sigma_y + c_3 \right)} \quad (10)$$

$$\left\{ \begin{array}{l} \mu_x : \text{the average of } x \\ \mu_y : \text{the average of } y \\ \sigma_x^2 : \text{the variance of } x \\ \sigma_y^2 : \text{the variance of } y \\ Cov_{xy} : \text{the covariance of } x \text{ and } y \end{array} \right. \quad \text{with} \quad \left\{ \begin{array}{l} c_1 = (k_1 L)^2 \\ c_2 = (k_2 L)^2 \\ c_3 = \frac{c_2}{2} \\ k_1 = 0,01 \\ k_2 = 0,03 \end{array} \right.$$

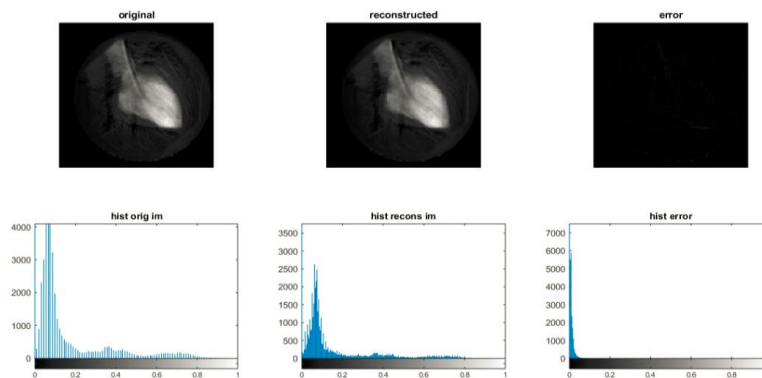
Where  $L$  is the dynamic of the image and is 255 for grayscale images

## 5 RESULTS AND DISCUSSION

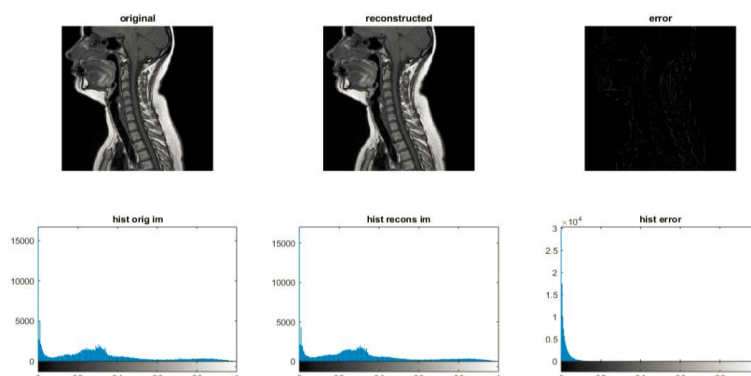
### 5.1 RESULTS

Our algorithm was applied to medical images. The quality of the reconstructed images after compression/decompression was evaluated by computational criteria such as the  $MSE$ , the  $PNSR$ , the  $IF$  and the  $SSIM$ . The results obtained are as follows:

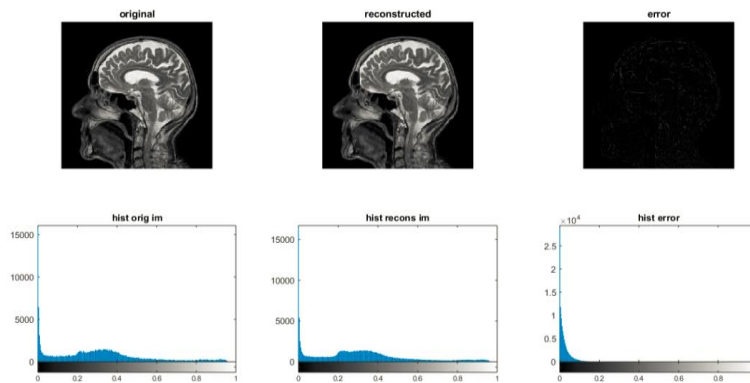
a) Heart



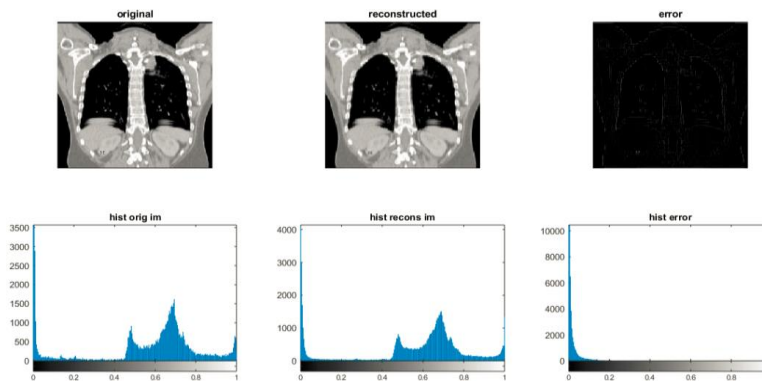
b) Cervical medical branch block



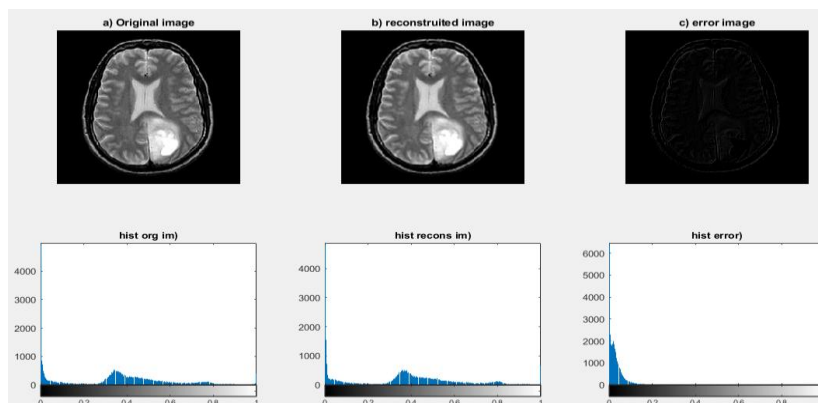
c) IRM



d) Respiratory CT Artifacts



e) Back plan of the brain



The evaluation of the quality of the images obtained after compression by computer criteria and the compression ratio are recorded in the following table:

Table 1. Algorithm evaluation parameters

N°	Image	Original image	PSNR	IF	CR(%)	MSE	SSIM
1	Back plan of the brain	184	38.095	0.96	85,700	9.852	0,87
2	Cervical IRM	397	37.031	0.88	91,127	12.588	0,93
3	Encephale IRM	202	35.415	0.81	94,401	18.685	0,90
4	echographic	129	34.851	0.79	95,794	21.280	0,64
5	Axial IRM	119	33.983	0.80	97,806	25.944	0,70
6	IRM brain	414	30.002	0.701	98,204	30.015	0,89
7	heart	34	32.556	0.783	97,409	3.011	0,91
8	mammographic	167	34.685	0.85	94,776	23.689	0,88
9	Encephalic IRM	90	30.989	0.632	99,036	30.540	0,86
10	Head injury	286	35.825	0.812	96,339	17.005	0,68

## 5.2 DISCUSSION

Table 1 above presents the results obtained by applying our algorithm to medical images. We can see that the fidelity between the original image and the compressed image varies between 0.632 and 0.96. This shows an almost insignificant difference between the original image and the compressed image. As far as the compression ratio is concerned, our algorithm obtains a ratio varying from 85 to 99. This constitutes a rather remarkable gain in space. Knowing that the MSE is a parameter for evaluating the quality of the image, our algorithm obtains an MSE varying between 9.85 and 30.540, proof of the performance of our algorithm. An evaluation of the quality of the reconstructed images after compression cannot be effective if the PSNR is not calculated. Through its high value, this parameter certifies the good quality of the image obtained after compression. The PSNR obtained by applying our algorithm to medical images shows that there is good conservation of the image energy, as its value varies between 30 and 38. Based on human visual perception, SSIM measures the structural similarity between the original image and the compressed image. This is a value between 0 and 1. A value of the structural similarity index between 0.6 and 1 demonstrates the effectiveness of the algorithm. Our algorithm records an SSIM oscillating between 0.64 and 0.93.

## 6 COMPARATIVE STUDY, ANOVA ANALYSIS AND INTERPRETATION

### 6.1 COMPARATIVE STUDY

In this subsection we will compare the skills of algorithms 1, 2 and 3. The idea is to evaluate their performance in terms of image quality obtained after compression. These performances were evaluated by computer parameters such as MSE and PSNR. For this, we have chosen some medical images with grayscale. The algorithms were performed in the same environment (MATLAB) at resolution  $j=2$  and we set the compression ratio to 60%.

The results of the comparison are listed in the table below;

Table 2. Compression results for both algorithms

N°	Images	Algorithm 3			Algorithm 2			Algorithm 1		
		CR	MSE	PSNR	CR	MSE	PSNR	CR	MSE	PSNR
1	brain	60	25,35	34,09	60	4.202	41.89	60	3.175	43.11
2	IRM-1	60	40,39	32,07	60	3.573	42.60	60	2.588	44.001
3	Encephale IRM	60	29,45	33,44	60	4.808	41.31	60	3.685	42.46
4	echographic	60	24.76	34,19	60	8.791	38.69	60	7.280	39.50
5	Axial IRM	60	37,19	32,43	60	7.320	39.48	60	6.944	39.71
6	IRM brain	60	20,39	35,03	60	7.220	39.54	60	4.415	41.68

With regard to this table, we come to the conclusion that the algorithm likely to be adopted in the medical field is algorithm 1. Because, for a compression ratio equal to 60%, it records the most important PSNR values compared to the other two

algorithms. As for the MSE, parameter measuring the degradation of the image after compression, algorithm 1 gets once more better result. These results presented in the table above thus reflect the capability of algorithm 1 provided a quality image after compression.

**6.2 ANALYSIS OF ANOVA RESULTS**

ANOVA (analysis of variance) is a statistical test to give the difference between the results while considering the differences of each algorithm. It also allows us to say whether the observed difference between the algorithms is significant or not. In other words, it will tell whether the results obtained by our algorithm are real and not due to chance. It is essential to specify that ANOVA is a statistical model used to compare the means of several algorithms  $n > 2$ . ANOVA is often associated with a so-called Fisher test. To perform the Fisher test it is necessary to check the following conditions:

- Independent observations (random selection of data considered);
- normally distributed data;
- no extreme data;
- variances of roughly equal groups;
- The number per group is about equal.

After validation of these conditions, two hypotheses are formulated:

- Hypothesis 1 generally noted  $H_0$ : this hypothesis suggests that the parameters of each algorithm are independent.
- Hypothesis 2 noted  $H_1$ : it however expresses the idea that the parameters are related.

The principle of the Fisher test is based on the comparison of the same variable between several algorithms. This study is based on the calculation of several variations:

- total variation: this is the variation observed within a group in relation to the group average:

$$SS_{total} = \sum_{i=1}^N (y_i - \bar{y})^2 \tag{11}$$

- intergroup variation: measures the variations of two averages between the different groups:

$$SS_{inter} = \sum_{j=1}^c (\bar{y}_j - \bar{y})^2 \tag{12}$$

- Intra-group variation: measures the magnitude of variation within a group:

$$SS_{intra} = \sum_{j=1}^c \sum_i^n (y_{i,j} - \bar{y})^2 \tag{13}$$

ANOVA measures the difference between  $SS_{inter}$  and  $SS_{intra}$ . The idea behind ANOVA is whether the gap is observed within a group or whether the gap is observed between groups. For this we calculate the parameter related to the following Fisher test:

$$F = \frac{\frac{SS_{inter}}{(c-1)}}{\frac{SS_{intra}}{(n-c)}} \text{ with } \begin{cases} n: \text{is the number of cases and} \\ c: \text{the number of category} \end{cases} \tag{14}$$

The value of F calculated in (14) will be compared to the theoretical F from Fisher Snedecor’s table.

- If  $F_{cal} < F_{th}$  then  $p - value < \alpha$ . The p-value, also called the probability value, is a statistical measure between 0 and 1. It is used for a hypothesis test. In addition, it is used to give an indication thus determining the quality of the observed results. The level of significance is generally defined as 5% (or 0.05). If it generates a p-value less than or equal to the significance level, the result is considered statistically significant (and rejects the null hypothesis). This is usually written as follows:  $p < 0.05$ . In this case  $H_0$  is rejected.
- ANOVA results

**Table 3. ANOVA table for the calculation of F**

Designation	Degree of freedom	Variance (Sum Sq)	Means of Sq (Mean Sq)	F value (F value)	P value Pr(>F)
Images	2	236.20	118.10	50.16	$2,27 \times 10^{-7}$
Residus	15	35.31	2.35	-	-

Note here that the overall probability associated with this test is  $2,27 \times 10^{-7}$ . This value is much less than 0,05 which means that there is a significant difference between the PSNR values from each algorithm. In other words, our data are significantly different.

Below we have the two-to-two comparison of each PSNR value obtained through the different algorithms used. This comparison will reveal the difference between the algorithms and the level of significance of this difference.

**Table 4. Highlighting the significance between the differences of the algorithms considered**

Differences	Estimation	Error	T value	$P_r( < t )$
Algo2 – Algo1	-1.1683	0.8859	-1.319	0.407
Algo2 – Algo3	-8.2017	0.8859	-9.258	<0.001
Algo3 – Algo1	-7.0333	0.8859	-7.939	<0.001

Note that the probability associated with the differences algo2-Algo3 and algo3-Algo1 is 0.001. This probability is well below 0.05 so the difference between these algorithms is very significant. On the other hand, the difference between algo2 and algo1 is very small because the probability associated with this difference is 0.407 which is much higher than 0.05.

Below is graphically representation of the differences between each algorithm.

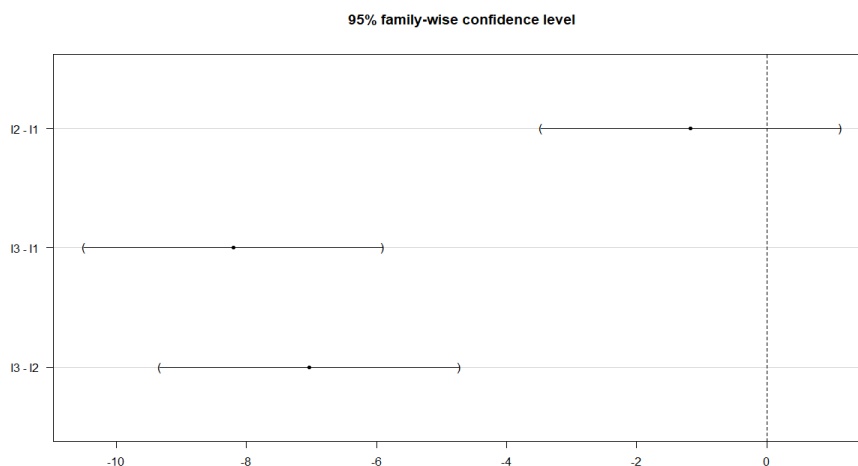


**Fig. 7. Difference in mean levels between algorithms.**

As mentioned above, the biggest difference is observed between algorithm 1 and algorithm 3.

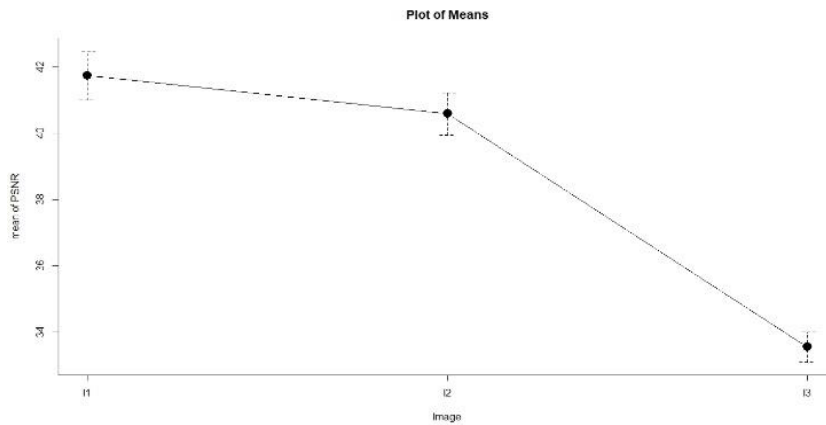


Fig. 8. Difference between algorithm averages.

The figure above shows the difference between the averages of the different algorithms used and once again algorithm 1 gets better result

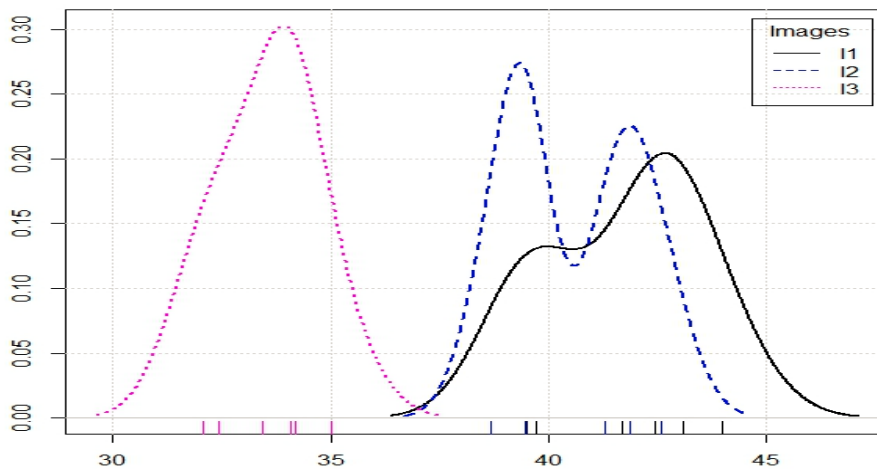


Fig. 9. Representation of the density of each algorithm according to the PSNR.

## 7 CONCLUSION

In this paper, a new algorithm for compression/decompression of grey-scale medical images was developed. To do so, an image decomposition was performed using the QWT formalism. Subsequently, we eliminated the coefficients of the sub-bands  $\omega_{LH,j}, \omega_{HL,j}$  and  $\omega_{HH,j}$  from  $j^{th}$  level of decomposition. After reconstruction of these sub-bands, we construct the orthogonal matrices  $A_{LH(j,p)}, B_{HL(j,p)}$  and  $C_{HH(j,p)}$  such that a matrix product with the sub-bands  $\omega_{LH,j}^1, \omega_{HL,j}^1$  and  $\omega_{HH,j}^1$  produces the matrices  $\omega_{LH,j}^{(11)}, \omega_{HL,j}^{(12)}$  and  $\omega_{HH,j}^{(13)}$ , most of whose coefficients are set to zero regardless of the singularity of the image. This algorithm not only provides a very good compression ratio, but also a very good quality of the image after reconstruction. Furthermore, our algorithm allows better preservation of the geometric structure of the image and to produce reconstructed images almost identical to the original image.

## REFERENCES

- [1] A.W. Wong, R. K. Taira, and H. K. Huang, Implementation of a digital archive system for a radiology department, in Proc. SPIE Conf. on Medical Imaging VI: PACS Design and Evaluation 1645, pp. 182-190, 1992.
- [2] H. Guitter, *La Compression des images numériques*, Edition Hermes, Paris, 1995.
- [3] C. Lucas, L. Urbano, R. Duvauferrier, B. Gibaud, D Cuvilliers ; J. M. Scarabin et A. Ramée, Evaluation surjective de la compression des images médicales, *Rev Im Med* (1992)4 : 53-59
- [4] Y.Y Chen, Medical image compression using DCT-based subband decomposition and modified SPIHT data organization, *international journal of medical informatics* 76 (2007) 717–725
- [5] Y. G. Wu et S. C. Tai, Medical Image Compression by Discrete Cosine Transform Spectral Similarity Strategy, VOL. 5, NO. 3, SEPTEMBER 2001
- [6] Woods et J.W. O'neil, Subband Coding, in *IEEE Transaction on Acoustics, Speech, and Signal Processing*, vol 34, n° 5, 1986.
- [7] J.R. Ordóñez, G. Gazuguel, J. Puentes, B. Solaiman et C. Roux, Indexation d'images médicales basée sur les informations spectrale et spatiale extraites de JPEG-2000, *Actes de CORESA'03, Lyon, 2003*.
- [8] Ruchika, M. Singh, A. R. Singh, Compression of Medical Images Using Wavelet Transforms, ISSN: 2231-2307, Volume-2, Issue-2, May 2012
- [9] N.Sathiyathan, A.Nagaraj, R. Karthick, medical image compression using view compensated wavelet transform, Volume 9, No. 9, September 2018
- [10] I.A Sawaneh, An Effective Method for e-Medical Data Compression Using Wavelet Analysis, Vol. 6, No. 3, 2018, pp. 25-32. doi: 10.11648/j.ijmi.20180603.12
- [11] K Gopi et T. R. Shri, Medical Image Compression Using Wavelets, Volume 2, Issue 4 (May. – Jun. 2013), PP 01-06
- [12] S. Boopathiraja et P. Kalavathi, A near lossless three-dimensional medical image compression technique using 3D-discrete wavelet transform, *Vol. 35, No. 3, 2021*
- [13] O.T Hui et R. Besar, medical image compression using jpeg-2000 and jpeg: a comparison study, Vol. 2, Nos. 3 & 4 (2002) 313-328
- [14] B.Perumal et M. P. Rajasekaran, A Hybrid Discrete Wavelet Transform with Neural Network Back Propagation Approach for Efficient medical Image Compression, 978-1-4673-6725-7/16/\$31.00 © 2016 IEEE
- [15] S. G. Miaou et S. C. Chen, A Lossless Compression Method for Medical Image Sequences Using JPEG-LS and Interframe Coding, VOL. 13, NO. 5, SEPTEMBER 2009
- [16] S. Valette, F. Thibon, Y. S. Kim, H. Y. Jung, I. Magnin et R. Prost, Décomposition en ondelettes de maillages triangulaires 3D irrégulièrement subdivisés. Application à la compression, GRETSI, 1999, Vannes, France. fihal-02272283ff, 2019
- [17] N. Benamrane, Z. B. Daho et J. Shen, compression des images médicales fixes par réseau de neurones, EL-Mnaouer 31000 Oran, Algérie, 2016
- [18] P. Anandan et R. S. Sabeenian, Medical Image Compression Using Wrapping Based Fast Discrete Curvelet Transform and Arithmetic Coding, Copyright © 2016 by authors and Scientific Research Publishing Inc.
- [19] S. Juliet, E. B Rajsingh et K. Ezra, A novel medical image compression using Ripplet transform, *J Real-Time Image Proc* (2016) 11:401–412, DOI 10.1007/s11554-013-0367-9, 2009
- [20] W. L. Chan, H. H. Choi, and R. G. Baraniuk. Coherent multiscale image processing using dual-tree quaternion wavelets. *IEEE Trans. Image Process.*, 17(7) :1069–1082, Jul. 2008.
- [21] B. Ledoux, E. Eloundou, A. J Oyobe, H. N Abena et P. Ele, compression of medical image using wavel quaterion transform, *international journal of Engineering &Technology*, 10(2) (2021) 89-94, 2021
- [22] C. Madhu, et E. Anant Shankar, Image Compression Using Quaternion Wavelet Transform, *Helix Vol. 8(1): 2691- 2695, 2017.*
- [23] W. L. Chan, H. Choi, and R. G. Baraniuk, Quaternion wavelets for image analysis and processing, In *Proc. IEEE Int'l Conf. on Image Processing*, pages 3057–3060, 2004.
- [24] R. Soulard, Quaternions et algèbres géométriques pour le traitement d'images, Master's thesis, University of Poitiers, 2009.
- [25] C. Madhu, E. Anant Shankar, « Image compression using Quaternion wavelet transform », *Helix vol. 8(1): 2691-2695, published on 31st December 2017, Copyright © 2018 Helix ISSN 2319 – 5592 (Online). <https://doi.org/10.29042/2018-2691-2695>.*